

# Gravitational Lensing and Dynamics in SL2S J02140-0535: Probing the mass out to large radius

T. Verdugo,<sup>1</sup> V. Motta,<sup>1</sup> R. P. Muñoz,<sup>1</sup> M. Limousin,<sup>2,3</sup> R. Cabanac,<sup>4</sup> J. Richard<sup>5</sup> \*

<sup>1</sup> Universidad de Valparaíso, Departamento de Física y Astronomía, Avenida Gran Bretaña 1111, Valparaíso, Chile

<sup>2</sup> Laboratoire d'Astrophysique de Marseille, Université de Provence,  
CNRS, 38 rue Frédéric Joliot-Curie, F-13388 Marseille Cedex 13, France

<sup>3</sup> Dark Cosmology Centre, Niels Bohr Institute, University of Copenhagen, Juliane Marie Vej 30, 2100 Copenhagen, Denmark

<sup>4</sup> Laboratoire d'Astrophysique de Toulouse-Tarbes, Université de Toulouse, CNRS, 57 Avenue d'Azereix, 65 000 Tarbes, France

<sup>5</sup> Durham University, Physics and Astronomy Department, South Road, Durham DH3 1LE, UK

Preprint online version: Submitted on ...

## ABSTRACT

**Context.** Studying the density profiles of galaxy groups offers an important insight into the formation and evolution of the structures in the universe, since galaxy groups bridges the gap between single galaxies and massive clusters.

**Aims.** We aim to probe the mass of SL2S J02140-0535, a galaxy group at  $z = 0.44$  from the Strong Lensing Legacy Survey (SL2S) which has uncovered this new population of group scale strong lenses.

**Methods.** We combine strong lensing modeling and dynamical constraints. The strong lensing analysis is based on multi-band HST/ACS observations which displays strong lensing features that we have followed up spectroscopically with VLT/FORS 2. In order to constrain the scale radius of an NFW mass profile not accessible to the lensing constraints, we propose a new method taking advantage of the large scale dynamical information provided by VLT/FORS 2 and KECK/LRIS spectroscopy of group members.

**Results.** In contrast with other authors, we have showed that the observed lensing features in SL2S J02140-0535 belongs to different background sources: one at  $z = 1.7 \pm 0.1$  (photometric redshift) yields three images while the other one at  $z = 1.0 \pm 0.06$  (spectroscopic and photometric redshift) is singly imaged only. Our unimodal NFW mass model reproduces very well these images. It is characterized by a concentration parameter  $c_{200} = 7.5 \pm 0.8$ , which is slightly greater than the value expected from  $\Lambda$ CDM simulations for its mass of  $M_{200} \approx 1 \times 10^{14} M_{\odot}$ . The spectroscopic analysis of group members also reveals a unimodal structure which do not present any evidence of merging. The position angle of the halo is  $\theta = 111.4 \pm 0.6$ , which is in agreement with the direction defined by the luminosity contours. We compare our dynamic mass estimate with independent weak lensing based mass estimate and we found that both are consistent, arguing for a relaxed galaxy group.

**Conclusions.**

**Key words.** Gravitational lensing: strong lensing – Galaxies: groups – Galaxies: groups: individual (SL2S J02140-0535)

## 1. Introduction

In the context of structure formation and evolution, galaxy groups play a key role, spanning the regime between individual galaxies and galaxy clusters. Therefore, detailed studies of this intermediate regime of the mass spectrum are relevant. Galaxy groups have been mostly studied using X-ray and optical tracers, as well as numerical simulations (*e.g.* Helsdon & Ponman 2000, 2003; Osmond & Ponman 2004; Willis et al. 2005; Finoguenov et al. 2007; Rasmussen & Ponman 2007; Mamon 2007; Faltenbacher & Mathews 2007; Yang et al. 2008; van den Bosch et al. 2008; Gastaldello et al. 2007; D'Onghia et al. 2005; Sommer-Larsen 2006, and references

*Send offprint requests to:* Tomas

\* Based on observations obtained with MegaPrime/MegaCam, a joint project of CFHT and CEA/DAPNIA, at the Canada-France-Hawaii Telescope (CFHT) which is operated by the National Research Council (NRC) of Canada, the Institut National des Sciences de l'Univers of the Centre National de la Recherche Scientifique (CNRS) of France, and the University of Hawaii. This work is based in part on data products produced at TERAPIX and the Canadian Astronomy Data Centre as part of the Canada-France-Hawaii Telescope Legacy Survey, a collaborative project of NRC and CNRS. Also based on HST data as well as Keck (LRIS) and VLT (FORS 2) data.

therein). Only recently, thanks to unsurpassed combined depth, area and image quality of the Canada France Hawaii Telescope Legacy Survey (CFHTLS)<sup>1</sup>, we have uncovered a new population of lenses, with Einstein radii between  $\sim 3''$  and  $\sim 8''$ , *i.e.* generated by galaxy-group scale-dark matter haloes (this subsample of the CFHTLS forms the Strong Lensing Legacy Survey<sup>2</sup> (SL2S), Cabanac et al. 2007). This new population effectively bridges the gap between single galaxies and massive clusters, opening a new window of exploration in the mass spectrum. The first representative sample of such lenses was recently presented by Limousin et al. (2009a). Since then, we are currently investigating in more details with the available data: SL2S J02176-0513 (Tu et al. 2009) and SL2S J08544-0121 (Limousin et al. 2009b). In this paper, we present an analysis of SL2S J02140-0535 at  $z = 0.44$ , combining strong and weak gravitational lensing, and dynamics of the group members.

Some researchers have demonstrated the advantages of joining different strong lensing regimes with the constraints that come from the stellar kinematics of the central brightest cluster galaxy (BCG). For example Sand et al. (2002, 2004) combined

<sup>1</sup> <http://www.cfht.hawaii.edu/Science/CFHTLS/>

<sup>2</sup> <http://www-sl2s.iap.fr/>

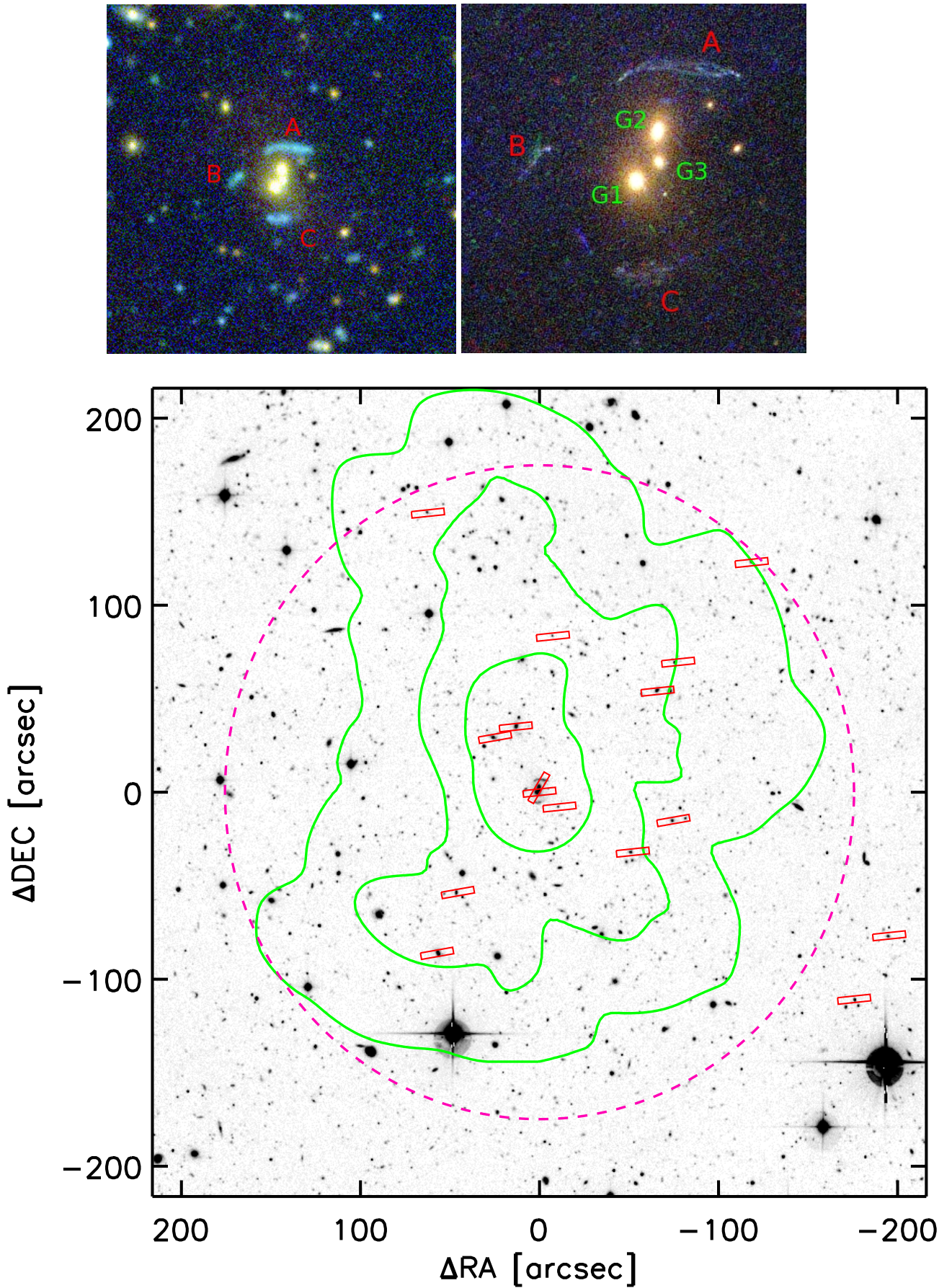


**Fig. 1.** The Group SL2S J02140-0532 at  $z_{\text{spec}} = 0.44$ . *Upper Left:* composite CFHTLS  $g, r, i$  colour image (1 square arcminute =  $343 \times 343$  kpc<sup>2</sup>). *Upper Right:* composite HST/ACS F814, F606, F475 colour image ( $22'' \times 22'' = 125 \times 125$  kpc<sup>2</sup>). Note how the space based image significantly improves the identification of multiple images and heightens the resolution allowing to detect the substructure. *Lower:* CFHTLS  $i$  band ( $7.2' \times 7.2' = 2.46 \times 2.46$  Mpc<sup>2</sup>) centred on the strong lensing system. We draw in green the luminosity contours (corrected for passive evolution) corresponding to  $10^5$ ,  $3 \times 10^5$ ,  $10^6$ ,  $3 \times 10^6$  and  $10^7$   $L_{\odot}$  kpc<sup>-2</sup>, respectively. Red rectangles show the location of the slits used for spectroscopy for the 16 confirmed members of the group and the magenta circle denotes a 1 Mpc distance from the centre of the group.

**Table 1.** Data of the galaxies and the arcs.

ID Name	X ["]	Y ["]	$u^* - g'$	$g' - i'$	$i' - r'$	$r' - z'$	$\epsilon$	$\theta_0$ [°]	$z$
G1	0.00	0.00	$2.35 \pm 0.11$	$1.61 \pm 0.02$	$0.86 \pm 0.01$	$0.36 \pm 0.01$	0.158	-41.0	$0.4446 \pm 0.0002$
G2	1.16	3.09	$2.99 \pm 0.23$	$1.64 \pm 0.03$	$0.87 \pm 0.01$	$0.37 \pm 0.01$	0.424	64.2	$0.4449 \pm 0.0003$
G3	1.37	1.25	$1.81 \pm 0.15$	$1.47 \pm 0.06$	$0.88 \pm 0.04$	$0.33 \pm 0.03$	0.177	18.26	—
A	—	—	$0.73 \pm 0.09$	$0.30 \pm 0.09$	$0.47 \pm 0.10$	$0.31 \pm 0.11$	—	—	[1.7 ± 0.1]
B	—	—	$0.60 \pm 0.11$	$0.07 \pm 0.11$	$0.39 \pm 0.14$	$0.36 \pm 0.14$	—	—	[1.7 ± 0.1]
C	—	—	$0.18 \pm 0.09$	$0.58 \pm 0.09$	$0.60 \pm 0.09$	$0.41 \pm 0.09$	—	—	[1.0 ± 0.06]

**Notes.** Column (1) list the identification for each object. Columns (2) and (3) list the relative positions measured with respect to the brightest group galaxy (BGG) with coordinates  $\alpha = 02:14:08:097$  and  $\delta = -05:35:33.77$ . Columns (4-7) lists the CFHTLS colors. Columns (8) and (9) show the geometric parameters: ellipticity  $\epsilon$  and position angle  $\theta_0$ , which gives the orientation of the semimajor axis from the horizontal line in the image, measured counterclockwise. In the last column we list the redshift; values in square brackets are photometric redshifts.

strong gravitational lensing with the velocity dispersion profile of the BCG and found that the models favored a shallower slopes in the NFW profiles. Recently, Newman et al. (2009) following the above works and adding weak lensing analysis, sampled the dark matter profile over three decades in radius in the lensing cluster Abell 611. Despite all these works, at group scales the efforts in that direction are just beginning. First, because strong lensing in groups is a relatively new field of research and second, due to observational limitations (few lensing arcs in groups and the fact that detecting weak lensing by groups of galaxies is challenging). Recently, McKean et al. (2010) probed the inner part of a group-scale halo using strong gravitational lensing and stellar kinematics and Thanjavur et al. (2010) showed that is possible to combine strong lensing and galaxy dynamics to characterize the mass distribution and the mass-to-light ratios of galaxy groups.

SL2S J02140-0535 was previously studied by Alard (2009) using a perturbative reconstruction of the gravitational lens. He found that the local shape of the potential and density of the lens, inferred from the perturbative solution, reveals the existence of an independent dark component that does not follow light. He argued that this particular shape of the dark halo is due to the merging of cold dark matter halos. Given these facts, the group represents a challenge, and then, to describe its mass distribution and perform a detailed study of the object have significant worth and deserves attention. Our first aim in this work is to build a strong lensing mass model for SL2S J02140-0535 using lensed features observed on HST/ACS data combined with ground based spectroscopy. The second one is to combine the strong lensing constraints with the dynamics of the groups members in order to study the mass profile up to the scale radius. And finally, we want to compare the masses obtained with the three methods, namely, strong lensing, weak lensing, and group dynamics; all with the purpose to shed some light to the study of SL2S J02140-0535.

The paper is organized as follows: In § 2, we describe the observational data image and spectroscopy and present the multiple images identification. In § 3, we define how the dynamical constraints (at galaxy scale and at group scale) enter in our strong lensing models. Also we depict the profiles for both, the group and the galaxy-scale mass components. In § 4, we present the strong lensing as well as the weak lensing analysis of SL2S J02140-0535 and the main results of the work. In § 5, we summarize and discuss our results. Finally in § 6, we present the

conclusions. All our results are scaled to a flat,  $\Lambda$ CDM cosmology with  $\Omega_M = 0.3$ ,  $\Omega_\Lambda = 0.7$  and a Hubble constant  $H_0 = 70 \text{ km s}^{-1} \text{ Mpc}^{-1}$ . All images are aligned with WCS coordinates, i.e. north is up, east is left. Magnitudes are given in the AB system.

## 2. Observations & Multiple Images Identification

SL2S J02140-0535 has been imaged both from ground and space based telescopes. From ground this group was observed in five filters ( $u^*$ ,  $g'$ ,  $r'$ ,  $i'$ ,  $z'$ ) as part of the CFHTLS using the wide field imager MEGAPRIME which covers  $\sim 1$  square degree on the sky, with a pixel size of  $0.186''$ . From space the lens was followed-up with the *Hubble Space Telescope* (HST). Observations were done in snapshot mode (C 15, P.I. Kneib) in three bands with the ACS camera (F814, F606 and F475). Moreover, a spectroscopic follow up of the arcs and the group members have been carried out from VLT and Keck.

### 2.1. Imaging

The strong lensing deflector in this group is populated by three galaxies (see Fig. 1 top left). The lensed images consist of three arcs surrounding the deflectors: one arc (labelled A) situated north of the deflector composed by two merging images, a second arc in the east (labelled B), and a third one (labelled C) in the south. Note that on this ground-based image, we see a possible image system consisting of ABC which seem to have compatible colors. In Fig. 1 (top right) we shows a color composition from the HST-ACS camera for the central part of the group. From the figure a new scenario emerge, could be possible that arc C is not associated with the proposed multiply image system, since it have different color. In addition, arc A presents some substructure that can also been appreciated in arc B. Given that Alard (2009) recently published an analysis based on this southern image being part of the multiply imaged system, special care will be used in order to properly assess the multiple image identification which is crucial for the analysis.

The photometry for the central galaxies labeled G1, G2 and G3 (see top right of Fig. 1), and for the arcs was performed in all CFHT bands with the IRAF package *apphot*. For the galaxies the magnitudes were derived by measuring fluxes inside a fixed circular aperture of 12 pixels ( $\sim 2.22''$ ) for galaxies G1 and G2, and 6 pixels ( $\sim 1.12''$ ) in galaxy G3. For the arcs we employed

polygonal apertures to obtain more accurate measurements. The vertices of the polygons for each arc were determined using the IRAF task polymark, and the magnitudes inside these apertures were calculated using the IRAF task polyphot.

The general properties of the central galaxies as well as the arcs are presented in Table 1. Column (1) list the identification for each object. Columns (2) and (3) list the relative positions measured with respect to the brightest group galaxy (BGG) with coordinates  $\alpha = 02:14:08:097$  and  $\delta = -05:35:33.77$ . Columns (4-7) lists the colors  $u^* - g'$ ,  $g' - r'$ ,  $r' - i'$  and  $i' - z'$ . Columns (8) and (9) show the geometric parameters derived from SExtractor (Bertin & Arnouts 1996): ellipticity  $\epsilon$  and position angle  $\theta_0$ , which gives the orientation of the semimajor axis from the horizontal line in the image, measured counterclockwise. Finally, column (10) list the redshifts (see the next subsections). Note in Table 1 that the colors  $u^* - g'$  and  $g' - r'$  for arc C differ significantly from the colors in A and B, which have (within the errors) almost similar values.

## 2.2. Spectroscopy

Two spectroscopic runs have been performed in the field of SL2S J02140-0532. Using LRIS (Oke et al. 1995) on Keck (Dichroic 680 and 560 nm, exposure 600s and 1200s with a slit of  $1.5''$ ), we have measured the redshifts of one of the brightest galaxies populating the strong lensing deflector (G2) and we found  $z = 0.4449 \pm 0.0003$ .

We also used FORS 2 on VLT (P.I. V. Motta) with a medium resolution grism (GRIS<sub>600RI</sub>) to target both group members and the strongly lensed features. Two masks were used and two exposures of 1400s were made with each mask. We selected the targets (other than strongly lensed features) as a two steps process. First we choose galaxies whose  $g - i$  color is within 0.15 from the  $g - i$  color of the two brightest galaxies populating the strong lensing deflector (see, Limousin et al. 2009a). Since the field was too crowded in the centre but not fully sampled at larger distances, we also picked all bright galaxies in the outer field whatever their color. Fig. 1 show the slits configuration for all confirmed group members. Full details on the spectroscopy of group members will be presented in a forthcoming publication (Muñoz et al., in prep.). Here we only concentrate on the spectroscopy of the lensed features.

No spectroscopic features were found in arcs A and B. On the other hand, the spectra of feature C reveals a strong emission line at  $7538\text{\AA}$ . As we can appreciate on Fig. 2 the emission line has a spatial extension that covers the whole arc. This line may come from [OII] $\lambda 3727$  at  $z = 1.0$  or Ly $\alpha$  at  $z = 5.2$ . However, the low redshift solution is much more likely and as we will discussed below, the photometric redshift estimate supports this conclusion. The presence of this line coming from the whole arc C is against the model of SL2S J02140-0535 presented in Alard (2009). He assumed that arcs A, B and C belong to the same source and he argued that the differences in colors observed in HST-ACS images was related to the crossing of the caustic line by a part of the source. His model predicts that one half of image C comes from the same part of the source as images A and B, but the other half corresponds an area of the source that has no counterpart in the large arcs (A and B). The lack of spectroscopic features in arcs A and B do not support this scenario.

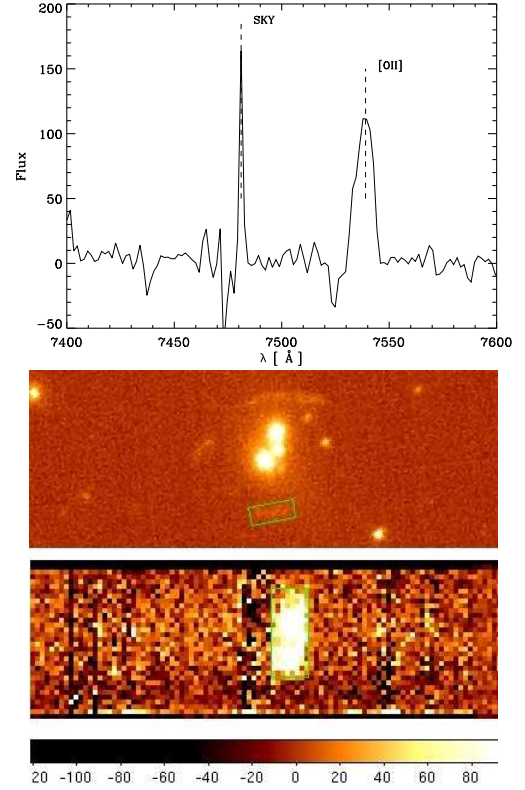


**Fig. 2.** *Top panel.* Spectrum of arc C. It shows a strong feature probably associated with [OII] $\lambda 3727$ . *Bottom panel.* VLT pre-image of SL2S J02140-0535 and the 2D spectrum of arc C. The green rectangle delineates the spatial extension of the feature in the 2D spectrum; as we can appreciate in the pre-image, the rectangle covers the whole arc.

## 2.3. Photometric Redshifts

Using the magnitudes reported in Table 1 we estimated the photometric redshifts for the features labelled A, B and C with the HyperZ software (Bolzonella et al. 2000). We present the output probability distribution function from HyperZ in Fig. 3. Arc C is constrained to be at  $z_{\text{phot}} = 1.0 \pm 0.06$ , which is in agreement with the identification of the emission line as being [OII] $\lambda 3727$  at  $z_{\text{spec}} = 1.0$ . The multiply imaged system constituted by Arc A and B has  $z_{\text{phot}} = 1.7 \pm 0.1$  and  $z_{\text{phot}} = 1.7 \pm 0.1$  respectively. Note, that although the probability distributions in the three cases are very broad (which is common in photometric redshift estimations using only five filters), there is not overlapping in the solutions below a  $3\sigma$  value, between system AB and arc C. Along with the similarity with the distributions of arc A and B, and the spectroscopic data, this ruled out the possibility that A, B and C belong to the same source.

## 2.4. Pixelizing the Arcs: increasing the number of constraints

When a source is mapped into a system that shows multiple sub-components (surface brightness peaks), like the one displayed by SL2S J02140-0535 (system AB), the number of constraints can be increased as well as the degree of freedom (for a fixed number of free parameters), since the peaks can be conjugated as different multiple images systems. In order to highlight the sub-structures appearing in system AB we subtracted the six central

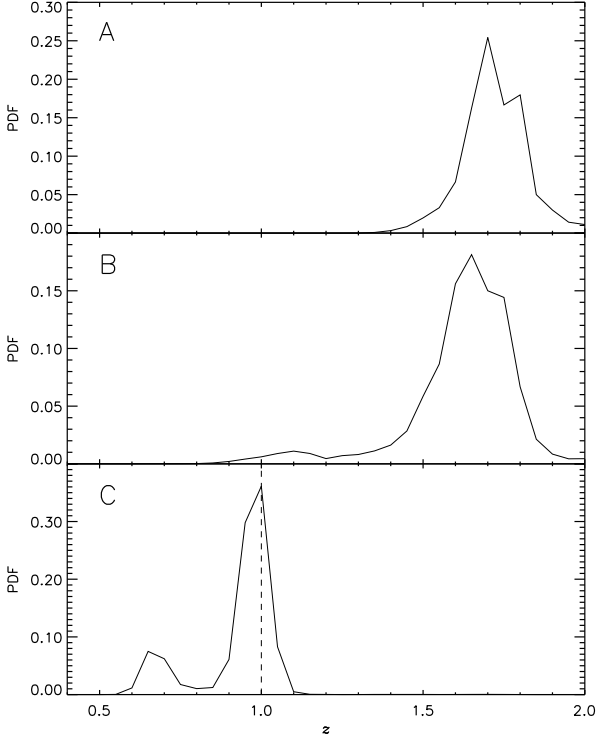


**Fig. 3.** Output photometric redshift PDF for arcs labelled A, B and C (top to bottom). The dashed vertical line corresponds to the spectroscopic inferred, assuming the emission line comes from [OII].

galaxies of the group (G1, G2, G3 and the three small ones near those, see Figure 1 top left). Following McLeod et al. (1998) we analyzed the F475W image and fitted a model convolved with a PSF. We used six de Vaucouleur profiles to fit the galaxies and a synthetic PSF because there was not a suitable non-saturated star in the field of view. To account for possible differences we additionally convolve the PSF with a Gaussian profile. In Fig. 4 we shows the central region of the group after the galaxy subtraction.

After an exhaustive analysis we conjugated some brightness peaks for which we were pretty confident in order to not introduce any bias in the modelling. This transforms our simple AB system in four different systems, 1.*i*, 2.*i*, 3.*i*, and 4.*i*, where *i* go from 1 to 3. In Fig. 4 we shows the image identification of the peaks, and in Table 2 we reported the positions (we assume that the typical uncertainties on the positions of identified conjugated images are 1 pixel  $\sim 0.05''$ ). To keep the same notation and to avoid confusion, we rename arc C as 5.1. Therefore, our model will have five different arc systems in the optimization procedure.

To summarize, we have shown that features presented in system AB are coming from the same background source which is multiply imaged. This background source at  $z_{\text{phot}} = 1.7 \pm 0.1$  yields three images in the image plane: arc A composed by two merging images and arc B. For each image, we have been able to conjugate substructures (systems 1.*i*, 2.*i*, 3.*i*, and 4.*i*). Besides, we have convincingly shown that arc C (now system 5.1) is a different object not multiple imaged.

### 3. Dynamical Constraints

In this section we describe the profiles used in our strong lensing models. Also we present how the dynamical constraints enter into the models at galaxy scale and at group scale.

#### 3.1. Galaxy Scale

We assume that the density profile of the stellar mass distribution in the central galaxies of SL2S J02140-0535 follows a Pseudo Isothermal Elliptical Mass Distribution (PIEMD). This profile was derived by Kassiola & Kovner (1993) and is parameterized by a central density  $\rho_0$ , linked to the central velocity dispersion,  $\sigma_0$ , which is related to the depth of the potential well (see Limousin et al. 2005; Elíasdóttir et al. 2007, for a detailed discussion of the properties of this mass profile). It is described using two characteristic radii that define changes in the slope of the density profile. In the inner region, the profile behaves like a non-singular isothermal profile with central density  $\rho_0$  and a core radius  $r_{\text{core}}$ . In the outer parts ( $r_{\text{cut}} < r$ ), the density progressively falls from  $\rho \propto r^{-2}$  to  $\rho \propto r^{-4}$ , introducing a natural cut-off. A clump modeled using PIEMD can be characterized using seven parameters: the center position, ( $X, Y$ ), the ellipticity  $\epsilon$ , the position angle  $\theta$  and the parameters of the density profile,  $\sigma_0$ ,  $r_{\text{core}}$ , and  $r_{\text{cut}}$ . Bellow, we will discuss the parameters associated with the dynamics of the central galaxies, namely,  $\sigma_0$  and  $r_{\text{cut}}$  and we shall return to the remaining in the next section.

Our spectroscopic data allow us to measure the redshift for two of the central galaxies in the group. However, given the bad quality in the galaxy G2 spectra (low S/N ratio), we only measured the line-of-sight internal velocity dispersion in galaxy G1. Using the penalized pixel-fitting method developed by Cappellari & Emsellem (2004) we found  $\sigma_{\text{los}} = 215 \pm 34 \text{ km s}^{-1}$  for the G-band absorption line profile. This velocity corresponds to  $\sigma_0^* = 253 \text{ km s}^{-1}$  (hereafter we denote with an asterisk quantities associated with galaxy G1) according to the relation reported by Elíasdóttir et al. (2007) who studied the internal velocity dispersion in some galaxies in Abell 2218 cluster.

Since the total stellar mass of the galaxy is related to  $\sigma_0^*$  and  $r_{\text{cut}}^*$  through the expression (Elíasdóttir et al. 2007):

$$M_* = \frac{1.5\pi}{G} r_{\text{cut}}^* \sigma_0^{*2}. \quad (1)$$

Then,  $r_{\text{cut}}^*$  can be constrained if we determine  $M_*$  in an independent way. In order to measure the stellar mass of Galaxy G1 we followed two different methods. First, we converted the *g* band magnitude into absolute rest frame V band luminosity and found  $L_V = 3.0 \times 10^{10} L_{\text{OV}}$ . Then we use the mass to light ratio reported in SLACS lenses (Gavazzi et al. 2007) to estimate the stellar mass and we found  $M_* \approx 1.0 \times 10^{11} M_{\odot}$ . For the second method, we employed the HyperZ software (Bolzonella et al. 2000) with the five magnitudes of Galaxy A reported in Table 1. We found a slightly greater value of  $M_* \approx 4.0 \times 10^{11}$ . Once we apply Eq. 1 these range of masses produce a range of possible values of  $r_{\text{cut}}^* = 1 - 6 \text{ kpc}$ .

The parameters of the remaining two galaxies are obtained using the following scale relations:

$$r_{\text{cut}} = r_{\text{cut}}^* \left(\frac{L}{L^*}\right)^{1/2}, \quad (2)$$

$$\sigma_0 = \sigma_0^* \left(\frac{L}{L^*}\right)^{1/4}.$$

Where  $\sigma_0^*$ ,  $r_{\text{cut}}^*$  and  $L^*$  are set with those values of galaxy A discussed above. For a discussion of these scaling relations we refer to Limousin et al. (2007).

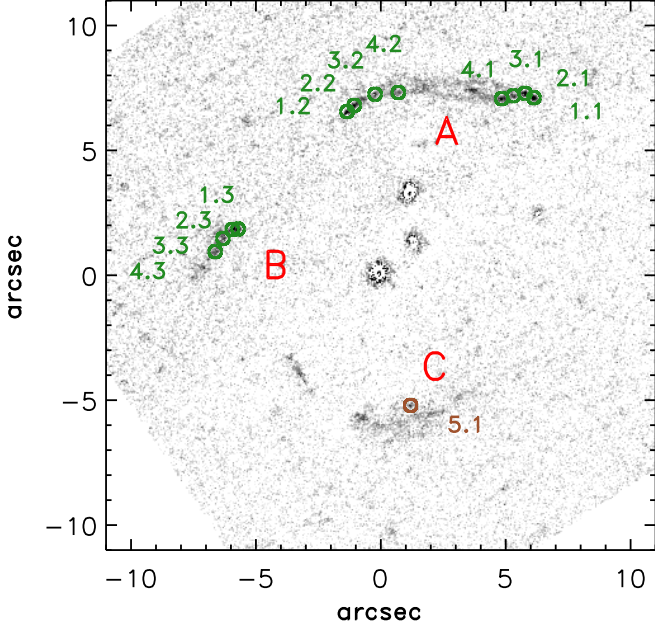


**Fig. 4.** F475W image ( $22'' \times 22''$ ) after the subtraction of the six central galaxies of the group. The green circles show the positions of the conjugated images that constitutes the arc system AB. The brown circle, mark the location of arc C.

**Table 2.** Multiple images identification.

Systems	$\alpha$ (J2000)	$\delta$ (J2000)
1.1	02:14:07.684	-05:35:27.37
1.2	02:14:08.184	-05:35:27.54
1.3	02:14:08.477	-05:35:31.68
2.1	02:14:07.708	-05:35:27.19
2.2	02:14:08.165	-05:35:27.32
2.3	02:14:08.493	-05:35:31.69
3.1	02:14:07.739	-05:35:27.26
3.2	02:14:08.110	-05:35:26.95
3.3	02:14:08.517	-05:35:32.00
4.1	02:14:07.770	-05:35:27.35
4.2	02:14:08.048	-05:35:26.93
4.3	02:14:08.538	-05:35:32.48
5.1	02:14:08.015	-05:35:38.54

## 3.2. Group Scale

### 3.2.1. Velocity dispersion and virial mass

In Fig. 5 we show the redshift distribution of the galaxies in the field of SL2S J02140-0535; as we can note, the spectroscopy reveals a well defined group without evidence of bimodality. The dynamical study of this group will be presented in a forthcoming publication (Muñoz et al. 2010 in preparation) as part of a detailed study of a sample of eight strong lensing galaxy groups in the SL2S. Here we will explain briefly the method used. We adopted the formalism by Wilman et al. (2005) in order to determine the group membership. We identified the group mem-

bers as follows: the group was initially assumed to be located at the redshift of the main bright lens galaxy,  $z_{lens}$ , with an initial observed-frame velocity dispersion of  $\sigma(v)_{obs} = 500(1+z_{lens}) \text{ km s}^{-1}$ . After computing the required redshift range for group membership and to applying a biweight estimator (Beers et al. 1990) the iterative process reach a stable membership solution with 16 secure members and  $\sigma = 630 \pm 107 \text{ km s}^{-1}$ . These galaxies are shown with red rectangles in the bottom of Fig. 1.

Assuming that the group has an isotropic velocity dispersion and that the cluster is no longer undergoing net expansion or contraction, we apply the virial theorem in order to estimate the mass of SL2S J02140-0535. From the equation  $M_v = 3R_v\sigma_{los}/G$  and using the measured  $\sigma_{los} = 363 \text{ km s}^{-1}$ , we obtained a mass of  $1.1 \pm 0.8 \times 10^{14} M_\odot$ . For a virial radius  $R_v = (\pi/2)R_H = 1.2 \pm 0.5 \text{ Mpc}$ , where  $R_H$  is the projected harmonic mean radius (e.g. Irgens et al. 2002). Although this is a great value for a mass in a galaxy group, we will see in the next section that is in agreement within the errors with our lensing results.

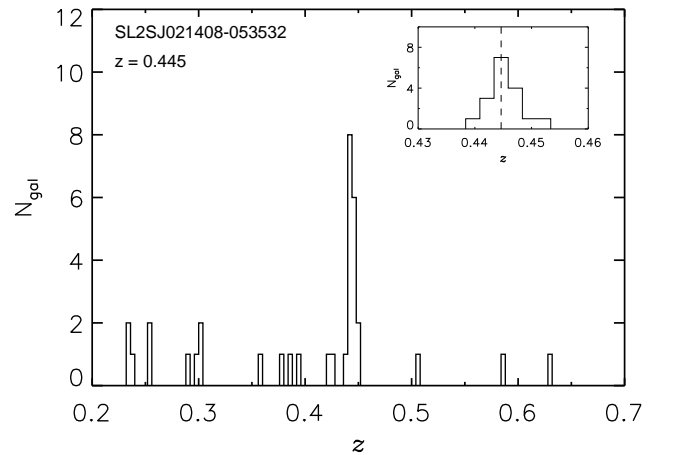


**Fig. 5.** The histogram (bin size  $\Delta = 0.004$ ) shows the redshift distribution along the direction of SL2S J0214-0535. The spectroscopic data reveals a well defined group at  $z = 0.444$ . The inset highlights the central part rebinned to  $\Delta = 0.0025$ . There are 17 galaxies in the histogram, however after the iterative algorithm (see text) one outlier was removed.

### 3.2.2. Dynamical constraints in the NFW profile

We will describe our galaxy group density profile as an NFW profile (Navarro et al. 1997):

$$\rho(r) = \frac{\rho_s}{(r/r_s)(1+r/r_s)^2} \quad (3)$$

where  $\rho_s$  is a characteristic density, and  $r_s$  is a scale radius that corresponds to the region where the logarithmic slope of the density equals the isothermal value. With the purpose of linking the velocity dispersion calculated in the last subsection with the velocity associated with the potential of the NFW halo, we follow Verdugo et al. (2007) and we define the velocity as:

$$\sigma^2 = \sigma_s^2 \equiv 4 \left( 1 + \ln \frac{1}{2} \right) G r_s^2 \rho_s \quad (4)$$

It is defined in such a way that it represents a realistic velocity dispersion and not only a scaling parameter (see the discussion in Verdugo et al. 2007).

Integrating Eq. 3 and using Eq. 4 we can express the virial mass in terms of velocity dispersion of the group and the scale radius:

$$M_v = \frac{\pi\sigma^2 r_s}{(1 + \ln \frac{1}{2})G} \left[ \ln(1 + R_v/r_s) - \frac{R_v/r_s}{1 + R_v/r_s} \right] \quad (5)$$

Then, given the virial mass and radius,  $M_v$ ,  $R_v$ , and the velocity dispersion of the group, we can use Eq. 5 to obtain the possible range of values for the scale radius. For  $M_v = 1.1 \pm 0.8 \times 10^{14} M_\odot$ ,  $R_v = 1.2 \pm 0.5$  Mpc, and  $\sigma = 630 \pm 107 \text{ km s}^{-1}$  we obtained that  $0 < r_s \leq 135$  kpc. This range is pretty broad, however we need to take into account the great errors bars in our measurements of the virial mass and radius. For the strong lensing analysis (see Section 4), we will use these dynamical results to put some priors in the range in which the parameters are allowed to vary: we set for the velocity dispersion the range given by its error,  $523 \text{ km s}^{-1} \leq \sigma_s \leq 737 \text{ km s}^{-1}$ , and for the scale radius we adopted  $50 \text{ kpc} \leq r_s \leq 135 \text{ kpc}$ , since values less than 50 kpc are very small for galaxy groups according to CDM simulations (e.g. Navarro et al. 1996).

## 4. Gravitational Lensing Analysis

### 4.1. Strong Lensing

For studying the lensing group SL2S J02140-0535, we used a parametric method as implemented in the LENSTOOL<sup>3</sup> ray-tracing code (Kneib 1993). This software use a Bayesian Monte Carlo Markov Chain (MCMC) method to search for the most likely parameters in the lens modeling (Jullo et al. 2007).

The identification of the multiply imaged system presented in Section 2 leads to 16 observational constraints. With these constraints, we computed a model (optimized in the image plane) with the following set of free parameters  $\{X, Y, \epsilon, \theta, r_s, \sigma, z_1, z_2, z_3, z_4, r_{cut}^*\}$ , where the first six parameters characterize the NFW profile and  $z_i$  represents the redshifts for the systems 1.i, 2.i, 3.i, and 4.i respectively. System 5.1, at  $z_{spec} = 1.0 \pm 0.06$  is used in the analysis as a singly imaged object. Multiple image systems were allowed to vary between 1.5 and 2.0 (approximately  $2\text{-}\sigma$  from the value inferred from the photometric redshift analysis) in order to take into account the broad PDF common in this measurements. The remaining parameters, those that describe the central galaxies, were set as follows: the center of the profiles are assumed to be the same as for the luminous components, and the ellipticity and position angle of the mass is assumed to be the same as those of the light. We use values reported in Table 1. The velocities dispersions are given trough Eq. 2 for a  $\sigma_0^* = 215 \text{ km s}^{-1}$ .

In Figure 6 we show the PDF for the arcs systems, and the best values obtained after the optimization. We obtained a mean best value of  $\bar{z} = 1.8 \pm 0.2$ , which agree within the errors with the estimated photometric redshifts. The results of our best fits are summarized in Table 3. In Figure 7 we show the predicted positions of our best model (orange and cyan squares), as well as the observed positions (green and brown circles). The remarkable agreement between both positions is quantified by a mean scatter in the image plane less than  $0.07''$ . While we have a  $\chi_{DOF}^2 = 2.8$ , this value is large since we are assuming a very small uncertainty on the positions of the images.

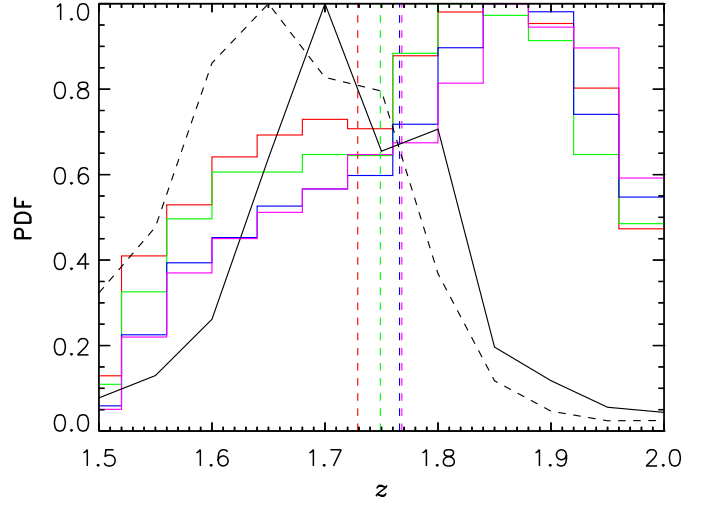


**Fig. 6.** Normalized PDFs. The red, blue, green and magenta histograms shows the distributions obtained with our first model, for  $z_1$ ,  $z_2$ ,  $z_3$  and  $z_4$  respectively. The vertical lines corresponds to the best model solutions given by the optimization procedure. Black continuous and black dashed lines are the distributions showed in Figure 3 for arcs A and B respectively.

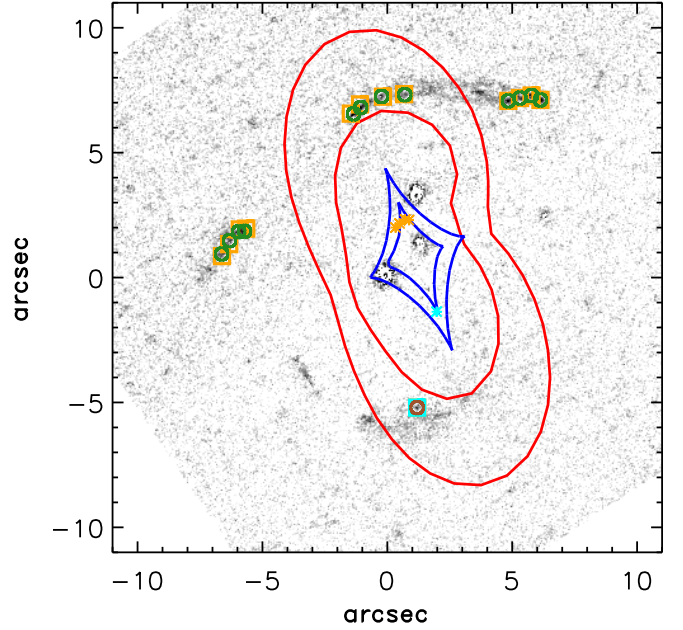


**Fig. 7.** Tangential critical lines (red) and caustic lines (blue) for two different sources located at  $z = 1.0$  and  $z = 1.8$ . As in Fig. 4 the circles show the measured positions of the images (input data for the model). The squares (orange and cyan) are the model-predicted image positions after optimization and the asterisks (orange and cyan) the positions in the source plane. Although the cyan asterisk appears to lay over the caustic line, this is only an artifact, product of the thick lines, and the size of the asterisks that we used to highlight the figure. The source is *not* over the caustic line.

<sup>3</sup> This software is publicly available at: <http://www.oamp.fr/cosmology/lenstool/>

## 4.2. Weak Lensing

The weak lensing analysis of this galaxy group has been performed in Limousin et al. (2009a). We refer the interested reader to that paper for a detailed description of our methodology, and we present below a brief summary. We select as background sources the galaxies whose  $i$  band magnitude falls between 21.5 and 24. Their density equals to  $13 \text{ arcmin}^{-2}$ . The completeness magnitude in this band equals to 23.96. Seeing equals to  $0.61''$ . A Bayesian method, implemented in the IM2SHAPE software (Bridle et al. 2002), is used to fit the shape parameters of the faint background galaxies and to correct for PSF smearing. From the catalogue of background galaxies, Limousin et al. (2009a) pursued a one dimensional weak lensing analysis. They fit a Singular Isothermal Sphere model (SIS) to the reduced shear signal between 150 kpc and 1.2 Mpc from the group centre, finding an Einstein radius equals to  $3.6 \pm 2.4''$ . In order to relate the strength of the weak lensing signal to a physical velocity dispersion characterising the group potential, Limousin et al. (2009a) estimate the mean geometrical factor using the photometric redshift catalogue from the T0004 release of the CFHTLS-Deep survey<sup>4</sup> (Ienna & Pelló 2006). They find  $\sigma_{\text{SIS}} = 612^{+180}_{-264} \text{ km s}^{-1}$ . This translates into a projected mass computed within a circular aperture of radius equals to 2 Mpc of  $5.5 \pm 3.7 \cdot 10^{14} M_{\odot}$ .

## 5. Discussion

Our best model show that it is possible to recover the observational features presented in the galaxy group SL2S J02140-0535, using a single halo for the group component plus three galaxy scale components associated with the central galaxies. We do not need extra assumptions about the mass distribution in the group. In addition, the position angle of the halo is oriented with a position angle well constrained at  $\theta = 111.4 \pm 0.6$ , which is the same direction as the one defined by the luminosity contours (Limousin et al. 2009a) and also is consistent with the spatial distribution of the confirmed members of the group (see Fig. 1 bottom).

The degeneracies in the  $\sigma$ - $r_s$  space are very common in strong lensing modeling (e.g. Jullo et al. 2007) since the region where the arcs appear is limited to the central region of the clusters and the scale radius is generally three or four times the distance to that region. Indeed, in galaxy groups this region is even smaller than in clusters. Then, is it not possible to constraint the scale radius of a group using only the strong lensing features observed in it. To highlight this behavior, we depicted in the top panel of Figure 8 the posterior PDFs for the  $\sigma$  and  $r_s$  parameters. Note how models with a scale radius greater than 135 kpc are still possible, however, we have set a limit to this value using information from the group dynamics. Thus, this give us a method that would be useful in order to break the degeneracies in the  $\sigma$ - $r_s$  space using the dynamics of the group obtained through spectroscopic data. It is important because provides a technique to fill the gap between strong lensing and weak lensing constraints in galaxy groups.

To further analyze the DM profile of SL2S J02140-0535, we calculated the concentration  $c_{200}$ , from the values  $r_s$  and  $\sigma$  (see the discussion in Verdugo et al. 2007). Here we assume that  $c_{200} = r_{200}/r_s$ , where we define  $r_{200}$  as the radius of a spherical volume within which the mean density is 200 times the critical density of the universe at the given redshift  $z$  of the group. In the bottom panel of Figure 8 we show the 2D histogram for the parameters  $c$  and  $r_s$ , we can note the same tendency with  $r_s$  as in

the top panel. Our best model give us a  $c_{200} = 7.5 \pm 0.8$ , which we can compare with a concentration defined as  $c = R_v/r_s$  using the values  $R_v = 1.2 \pm 0.5 \text{ Mpc}$ , and  $r_s = [0, 135] \text{ kpc}$  obtained in Section 4, however given these large errors it is clear that both values will match within the errors. On the other hand, we can compare with the values expected from  $\Lambda$ CDM numerical simulations. From the work of Neto et al. (2007), a DM halo with  $M_{200} \approx 1 \times 10^{14} M_{\odot}$  have  $c_{200} = 5.2 \pm 1.1$ , which agree within  $2\sigma$  with the value obtained for our group.

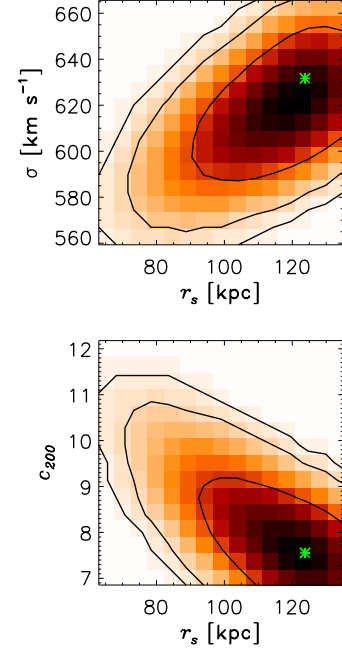


**Fig. 8.** PDFs of the parameters  $\sigma$ ,  $c_{200}$  and  $r_s$ . The three contours stand for the 68%, 95% and 99% confidence levels. The values obtained for our best model are marked by a green asterisk.

Given the relatively smaller mass of galaxy groups (compared with clusters) we do not expect to get a weak lensing signal enough to allow us to fully probe a NFW profile. Indeed, until the work of (Limousin et al. 2009a) weak lensing signals of such mass scales had been recovered only by stacking groups (e.g. Mandelbaum et al. 2006). However, the strength of the signal in SL2S J02140-0535 is sufficient to fit a SIS and to obtain the projected mass as a function of the radius. In Figure 9 we show the comparison between the masses obtained with the different methods exposed in the present work: Strong Lensing (green), Weak Lensing (blue) and the virial mass (red). As we constrained the mass profile up to the scale radius ( $r_s = 124 \pm 15 \text{ kpc}$ ), beyond this value we are extrapolating the strong lensing mass. From Figure 9 we can note that the masses are in agreement within the errors in the range  $0.7 \text{ Mpc} \leq r \leq 0.9 \text{ Mpc}$ .

*Comparison with Alard (2009)* - Using a perturbative method Alard (2009) reconstructed the structure and potential of the gravitational lens SL2S J02140-0535. In his work he assumed that arcs A, B and C belong to the same source. He argued that the differences in colors observed in HST-ACS images were related to the crossing of the caustic line by part of the source. His model predicts that one half of image C comes from the same part of the source as images A and B, but the other half corresponds an area of the source that has no counterpart in the large

<sup>4</sup> [http://www.ast.obs-mip.fr/users/rosier/CFHTLS\\_T0004/](http://www.ast.obs-mip.fr/users/rosier/CFHTLS_T0004/)

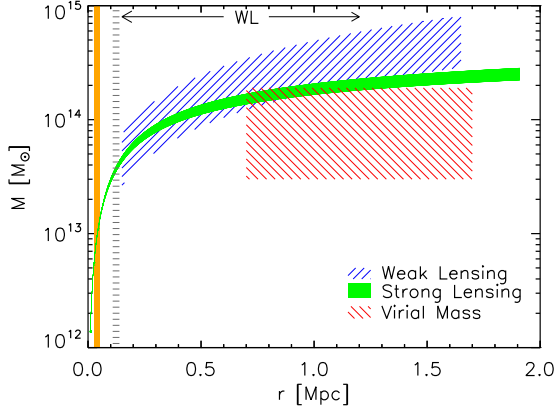


**Fig. 9.** The projected mass as a function of the aperture radius measured from the BGG. The green shaded area and blue region filled with lines corresponds to the mass profile within  $1\sigma$  errors for the strong lensing and the weak lensing models respectively. The red region filled with lines illustrates the virial mass derived from the dynamic analysis. The orange shaded region show the area where lies the arcs systems and the gray region filled with lines the model-predicted scale radius. Also we depicted an arrow to illustrate the zone of the weak lensing signal.

arcs (A and B). The perturbative method is capable of reproducing such arc configuration, however the model predicts the existence of an independent dark component that does not follow light. In the present work, we have demonstrated that system AB and system C belong to different sources, one at  $z = 1.7 \pm 0.1$  and the other one at  $z = 1.0 \pm 0.06$ . Our model, with a single NFW profile (which is consistent with the analysis of the luminosity contours (Fig. 1 bottom) and the redshift distribution of the galaxies in the field of SL2S J02140-0535 (see Fig. 5)), can fit the arcs features observed in the group and our results point out that the projected light of the group traces the dark matter distribution.

## 6. Conclusions

We have probed the gravitational potential of SL2S J02140-0535 on a large radial range using complementary techniques: strong lensing, weak lensing and dynamics. In the strong lensing regime we performed a fit using an NFW profile and three Galaxy-scale mass components as perturbations to the group potential. We used PIEMDs for the individual galaxies and set constraints to their geometrical and dynamical parameters using observational data (image and spectroscopy). We measured the velocity dispersion of the group using Keck (LRIS) and VLT (FOR2) spectra, and we apply this information in order to constrain and to build a reliable strong lensing model based on one multiply imaged system and one single image system. In the weak lensing regime, we use the analysis reported in Limousin et al. (2009a). Our main results can be summarized as follows:

1. We have showed that system AB and system C belong to different sources, one at  $z = 1.7 \pm 0.1$  (photometric redshift) and the other one at  $z = 1.0 \pm 0.06$  (spectroscopic and photometric redshift) respectively.
2. The velocity dispersion provide constraints on the scale radius of the NFW profile. In the present work we show that

is possible to use the dynamics at group scale in order to discriminate between a great range of possible  $r_s$  values. In particular, we found  $r_s = 124 \pm 15$  kpc. This scale radius with the velocity dispersion found for our best model,  $\sigma = 632 \pm 17$ , gives a concentration value  $c_{200} = 7.5 \pm 0.8$  which is slightly greater than the one predicted by  $\Lambda$ CDM simulations.

3. Our best lens model reproduced quite well the image systems observed in the field of SL2S J02140-0535, with no extra assumptions about the underlying mass distribution (e.g. bimodal distribution). This is in agreement with the spectroscopic analysis that shows a well defined group. Furthermore, we obtained a position angle of the halo of  $\theta = 111.4 \pm 0.6$ , that is consistent with the orientation of the luminosity contours and the spatial distribution of confirmed members.
4. The masses obtained with Strong Lensing, Weak Lensing and the virial mass estimated from the velocity dispersion of the group agree within the errors. Thus we demonstrated that is possible to join these three different methodologies to get a complete insight in the mass of a galaxy group.

The lensing and dynamical analysis of SL2S J02140-0535 presented in this paper, stand out two principal points. First, the impact of including spectroscopic information of arcs (i.e. with secure arcs identifications) in strong lensing models in order to avoid complex mass distribution models that does not follow the light. Two, the possibility to settle large scale properties not accessible through Strong Lensing, as the scale radius in the NFW profile. Future spectroscopic follow-up of the arcs A and B will provide a confirmation test for our model. In addition, deepest HST images of the group will allow us to construct a better weak lensing models capable to probe an NFW profile at large scales, as well as to improve our strong lensing model.

*Acknowledgements.* T. Verdugo acknowledge support from FONDECYT through grant 3090025. T. Verdugo thank the Laboratoire d'Astrophysique de Marseille and the Institut d'Astrophysique de Paris for the two kindly invitations to work in their facilities. VM acknowledges partial support from FONDECYT 1090673 and DIPUV 09/2007. RPM acknowledges partial support from CONICYT CATA-BASAL and Comité Mixto ESO-Gobierno de Chile. ML thanks the Centre National d'Etudes Spatiales (CNES) and CNRS for their support. ML est bénéficiaire d'une bourse d'accueil de la Ville de Marseille. The Dark Cosmology Centre is funded by the Danish National Research Foundation. JR acknowledges support from a EU Marie-Curie fellowship.

## References

- Alard, C. 2009, *A&A*, 506, 609  
 Beers, T. C., Flynn, K., & Gebhardt, K. 1990, *AJ*, 100, 32  
 Bertin, E. & Arnouts, S. 1996, *A&A*, 117, 393  
 Bolzonella, M., Miralles, J.-M., & Pelló, R. 2000, *A&A*, 363, 476  
 Bridle, S., Kneib, J.-P., Bardeau, S., & Gull, S. 2002, in *The shapes of galaxies and their dark halos*, Proceedings of the Yale Cosmology Workshop, New Haven, Connecticut, USA, 28-30 May 2001. Edited by Priyamvada Natarajan., ed. P. Natarajan, 38+  
 Cabanac, R. A., Alard, C., Dantel-Fort, M., et al. 2007, *A&A*, 461, 813  
 Cappellari, M. & Emsellem, E. 2004, *PASP*, 116, 138  
 D'Onghia, E., Sommer-Larsen, J., Romeo, A. D., et al. 2005, *ApJ*, 630, L109  
 Elíasdóttir, Á., Limousin, M., Richard, J., et al. 2007, *ArXiv e-prints*, 710  
 Faltenbacher, A. & Mathews, W. G. 2007, *MNRAS*, 375, 313  
 Finoguenov, A., Ponman, T. J., Osmond, J. P. F., & Zimer, M. 2007, *MNRAS*, 374, 737  
 Gastaldello, F., Buote, D. A., Humphrey, P. J., et al. 2007, *ApJ*, 669, 158  
 Gavazzi, R., Treu, T., Rhodes, J. D., et al. 2007, *ApJ*, 667, 176  
 Helsdon, S. F. & Ponman, T. J. 2000, *MNRAS*, 315, 356  
 Helsdon, S. F. & Ponman, T. J. 2003, *MNRAS*, 339, L29  
 Jenna, F. & Pelló, R. 2006, in *SF2A-2006: Semaine de l'Astrophysique Française*, ed. D. Barret, F. Casoli, G. Lagache, A. Lecavelier, & L. Pagani, 347+–

- Irgens, R. J., Lilje, P. B., Dahle, H., & Maddox, S. J. 2002, *ApJ*, 579, 227
- Jullo, E., Kneib, J.-P., Limousin, M., et al. 2007, *New Journal of Physics*, 9, 447
- Kassiola, A. & Kovner, I. 1993, *ApJ*, 417, 450
- Kneib, J.-P. 1993, PhD thesis, Université Paul Sabatier, Toulouse III, France
- Limousin, M., Cabanac, R., Gavazzi, R., et al. 2009a, *A&A*, 502, 445
- Limousin, M., Jullo, E., Richard, J., et al. 2009b, *ArXiv e-prints*
- Limousin, M., Kneib, J.-P., & Natarajan, P. 2005, *MNRAS*, 356, 309
- Limousin, M., Richard, J., Jullo, E., et al. 2007, *ApJ*, 668, 643
- Mamon, G. A. 2007, in *Groups of Galaxies in the Nearby Universe*, ed. I. Saviane, V. D. Ivanov, & J. Borissova, 203–+
- Mandelbaum, R., Seljak, U., Cool, R. J., et al. 2006, *MNRAS*, 372, 758
- McKean, J. P., Auger, M. W., Koopmans, L. V. E., et al. 2010, *MNRAS*, 317
- McLeod, B. A., Bernstein, G. M., Rieke, M. J., & Weedman, D. W. 1998, *AJ*, 115, 1377
- Navarro, J. F., Frenk, C. S., & White, S. D. M. 1996, *ApJ*, 462, 563
- Navarro, J. F., Frenk, C. S., & White, S. D. M. 1997, *ApJ*, 490, 493
- Neto, A. F., Gao, L., Bett, P., et al. 2007, *MNRAS*, 381, 1450
- Newman, A. B., Treu, T., Ellis, R. S., et al. 2009, *ApJ*, 706, 1078
- Oke, J. B., Cohen, J. G., Carr, M., et al. 1995, *PASP*, 107, 375
- Osmond, J. P. F. & Ponman, T. J. 2004, *MNRAS*, 350, 1511
- Rasmussen, J. & Ponman, T. J. 2007, *MNRAS*, 380, 1554
- Sand, D. J., Treu, T., & Ellis, R. S. 2002, *ApJ*, 574, L129
- Sand, D. J., Treu, T., Smith, G. P., & Ellis, R. S. 2004, *ApJ*, 604, 88
- Sommer-Larsen, J. 2006, *MNRAS*, 369, 958
- Thanjavur, K., Crampton, D., & Willis, J. 2010, *ArXiv e-prints*
- Tu, H., Gavazzi, R., Limousin, M., et al. 2009, *A&A*, 501, 475
- van den Bosch, F. C., Pasquali, A., Yang, X., et al. 2008, *ArXiv e-prints* 0805.002
- Verdugo, T., de Diego, J. A., & Limousin, M. 2007, *ApJ*, 664, 702
- Willis, J. P., Pacaud, F., Valtchanov, I., et al. 2005, *MNRAS*, 363, 675
- Wilman, D. J., Balogh, M. L., Bower, R. G., et al. 2005, *MNRAS*, 358, 71
- Yang, X., Mo, H. J., & van den Bosch, F. C. 2008, *ApJ*, 676, 248

**Table 3.** Best-fitting parameters.

Comp.	X [ $''$ ]	Y [ $''$ ]	$\epsilon$	$\theta$ [ $^\circ$ ]	$r_{core}$ [kpc]	$r_s$ [kpc]	$r_{cut}$ [kpc]	c	$\sigma_0$ [km s $^{-1}$ ]	$\sigma$ [km s $^{-1}$ ]	$\chi^2_{DOF}$
Group	$1.3 \pm 0.1$	$0.6 \pm 0.3$	$0.27 \pm 0.01$	$111.4 \pm 0.6$	—	$124 \pm 15$	—	$7.5 \pm 0.8$	—	$632 \pm 17$	2.8
$L^*$	—	—	—	—	[0.15]	—	$3.4 \pm 0.8$	—	[253]	—	

**Notes.** The first column identifies the different scale components. The  $L^*$  denotes the galaxy-scale mass component. Columns 2 and 3 list the position in arcseconds relative to the BGG. Columns 4 and 5 the geometric parameters. From columns 6 to 11 the different profiles parameters. In the last column the  $\chi^2_{DOF}$ . Values in square brackets are not optimized.